A Dwarf Galaxy Debris Stream Associated with Palomar 1 and the Anticenter Stream

Yong Yang[1,2] , Jing-Kun Zhao[1] , Xian-Hao Ye[1,2] , Gang Zhao[1,2] , and Ke-Feng Tan[1]

[1] CAS Key Laboratory of Optical Astronomy, National Astronomical Observatories, Chinese Academy of Sciences, Beijing 100101, People's Republic of China
zjk@bao.ac.cn
[2] School of Astronomy and Space Science, University of Chinese Academy of Sciences, Beijing 100049, People's Republic of China

Abstract

We report the discovery of a new stream (dubbed as Yangtze) detected in Gaia Data Release 3. The stream is at a heliocentric distance of $\sim$9.12 kpc and spans nearly $27°$ by $1°.9$ on the sky. The color–magnitude diagram of Yangtze indicates a stellar population of age $\sim$11 Gyr and $[M/H] \sim -0.7$ dex. It has a number density of about 5.5 stars deg^{-2} along with a surface brightness of $\Sigma_G \simeq 34.9$ mag arcsec^{-2}. The dynamics and metallicity estimate suggest that Yangtze may be closely related to Palomar 1 and the Anticenter Stream.

Unified Astronomy Thesaurus concepts: Milky Way stellar halo (1060); Stellar streams (2166)

1. Introduction

The Milky Way has proven to be full of substructures either embedded in the disk (e.g., Zhao et al. 2009; Liang et al. 2017; Antoja et al. 2018; Zhao et al. 2018; Re Fiorentin et al. 2021; Yang et al. 2021; Ye et al. 2021; Zhao & Chen 2021) or hidden in the halo (e.g., Ibata et al. 1994; Newberg et al. 2009; Law & Majewski 2010; Grillmair & Carlin 2016; Helmi et al. 2018; Zhao et al. 2020; Ibata et al. 2021; Yang et al. 2022c; Mateu 2023). Identifying and studying them can help us better understand the current status as well as the past story of our Galaxy, which is especially true for stellar streams formed from the disruption of satellite galaxies. This type of stream records accretion events that reveal the formation history of the Milky Way. They have also maintained spatial clustering properties that make it possible to probe their kinematics and dynamics by tracing orbits (e.g., Chang et al. 2020; Malhan et al. 2021). However, unlike globular-cluster-origin streams, the number of known dwarf galaxy streams is still limited so far (e.g., Sagittarius, Ibata et al. 1994; Orphan, Grillmair 2006a; Cetus, Newberg et al. 2009; Tucana III, Li et al. 2018; LMS-1, Yuan et al. 2020). Thus searching for this type of stream is of great importance and necessity.

In this Letter, we report on the detection of a dwarf galaxy debris stream that we designate Yangtze. The stream is exposed when we weight stars in a color–magnitude diagram (CMD) and proper motions (PMs) simultaneously using Gaia Data Release 3 (DR3; Gaia Collaboration et al. 2021; Lindegren et al. 2021; Riello et al. 2021). Section 2 describes the detecting strategy, and Section 3 characterizes the stream. A conclusion is given in Section 4.

2. A Stream Scanner

To search for streams of the Galactic halo, stars from Gaia DR3 with galactic latitude $|b| > 15°$ are retrieved. In order to ensure good astrometric and photometric solutions, only stars with a renormalized unit weight error < 1.4 and $|C^*| < 3\sigma_{C*}$ are retained, where C^* is the corrected blue photometer (BP) and red photometer (RP) flux excess factor that was introduced

by Riello et al. (2021) to identify sources for which the G-band photometry and BP and RP photometries are not consistent.

A modified matched-filter technique has been adopted in Grillmair (2019) and Yang et al. (2022a) to search for the tidal streams extended from globular clusters (GCs). The technique weights stars using their color differences from the cluster's locus in the CMD. These weights are further scaled based on the stars' departures from PMs of the cluster's orbit. Nevertheless, the limitation is that we must know the location and velocity of the progenitor such that we can integrate its orbit along which we assign weights to stars. In this work, we improve this method to make it applicable even if there is no prior knowledge about the stream progenitor.

In the CMD, we use an isochrone of old and metal-poor stellar population (e.g., age = 13 Gyr and $[M/H] = -2.2$ dex) extracted from the Padova database (Bressan et al. 2012) as the filter. Individual stars are assigned weights based on their color differences from the isochrone, assuming a Gaussian error distribution:

$$w_{CMD} = \frac{1}{\sqrt{2\pi}\,\sigma_{color}} \exp\left[-\frac{1}{2}\left(\frac{color - color_0}{\sigma_{color}}\right)^2\right]. \quad (1)$$

Here color and σ_{color} denote BP−RP and corresponding errors, respectively. σ_{color} is simply calculated through $\sqrt{\sigma_{BP}^2 + \sigma_{RP}^2}$, where σ_{BP} and σ_{RP} are obtained with a propagation of flux errors (see the CDS website[3]). $color_0$ is determined by the isochrone at a given G magnitude of a star. All stars have been extinction corrected using the Schlegel et al. (1998) maps as recalibrated by Schlafly & Finkbeiner (2011) with RV = 3.1, assuming $A_G/A_V = 0.83627$, $A_{BP}/A_V = 1.08337$, and $A_{RP}/A_V = 0.63439$.[4] Therefore, w_{CMD} is a function of distance modulus (*dm*) once the isochrone is selected. In terms of PMs,

---

[3] https://vizier.u-strasbg.fr/viz-bin/VizieR-n?-source=METAnot&catid=1350&notid=63&-out=text
[4] These extinction ratios are listed on the Padova model site: http://stev.oapd.inaf.it/cgi-bin/cmd.

weights are computed as

$$w_{\rm PMs} = \frac{1}{2\pi\sigma_{\mu_\alpha^*}\sigma_{\mu_\delta}}$$

$$\times \exp\left\{-\frac{1}{2}\left[\left(\frac{\mu_\alpha^* - \mu_{\alpha,0}^*}{\sigma_{\mu_\alpha^*}}\right)^2 + \left(\frac{\mu_\delta - \mu_{\delta,0}}{\sigma_{\mu_\delta}}\right)^2\right]\right\}. \quad (2)$$

Here μ_α^*, μ_δ, $\sigma_{\mu_\alpha^*}$, and σ_{μ_δ} are measured PMs and corresponding errors of stars. $\mu_{\alpha,0}^*$ and $\mu_{\delta,0}$ are two variables of $w_{\rm PMs}$ varying in the PM space.

Finally, star weights are obtained by $w = w_{\rm CMD} \times w_{\rm PMs}$, which is a function of dm, $\mu_{\alpha,0}^*$, and $\mu_{\delta,0}$ (i.e., $w = w(dm, \mu_{\alpha,0}^*, \mu_{\delta,0})$). We calculate w for all stars over a grid of the three variables: dm from 11.5 to 17.5 mag with a step of 0.2 mag, $\mu_{\alpha,0}^*$ from -15 to 15 mas yr^{-1}, and $\mu_{\delta,0}$ from -20 to 10 mas yr^{-1}, both with a step of 1 mas yr^{-1}.[5] At each grid point, the stars' weights are summed in sky pixels to expose structures. We refer to this method as `StreamScanner`[6] later because what it is doing is like scanning streams in the CMD and PM spaces.

`StreamScanner` is a simple and direct way that relies on measurements from observation and does not need too-complicated assumptions or models. We happen to find the signature of Yangtze in this work when `StreamScanner` is placed at $(dm, \mu_{\alpha,0}^*, \mu_{\delta,0}) = (13.7, -1, 1)$. We then refine these parameters along with a choice of the isochrone as elaborated in Section 3.

3. The Yangtze Stream

A weighted sky map is obtained as shown in the middle panel of Figure 1. This is a coadded result of $w(14.8, -0.4, 0.8)$ and $w(14.8, -1, 1.4)$ using an isochrone with age = 11 Gyr and [M/H] = -0.7 dex, where the isochrone and its dm are determined by a CMD fit to the stream (see Section 3.1), and the choices of $(\mu_{\alpha,0}^*, \mu_{\delta,0})$ are based on Figure 3. The sky pixel width is 0°.2, and the coadded map is smoothed with a Gaussian kernel of $\sigma = 0°.4$. The stretch is logarithmic, with brighter areas corresponding to higher-weight regions. The white area in the bottom left corner is due to the proximity to the Galactic disk. Furthermore, only stars fainter than $G = 18$ mag (corresponding to the stream's main-sequence turnoff; see Figure 3) are shown here because random, brighter field stars might introduce large noises due to their rather low photometric and astrometric uncertainties. In the left and right panels, we further plot the dust extinction map extracted from Schlegel et al. (1998) and Gaia's scanning pattern covered by the DR3, respectively, with higher values represented by darker colors. The red dashed line in the three panels indicates the trajectory of Yangtze.

From the matched-filter map, the signature of Yangtze starts at $\delta = -13°$ and ends at $\delta = 14°$. In addition, there are several random noises appearing around the stream, which do not represent actual physical overdensities. According to the other two panels, we can verify that the stream does not follow any structures in the interstellar extinction and is not aligned with any features in Gaia's scanning pattern. Although there is a small region at $\delta \sim 0°$ where dust might be heavy, it does not

resemble the stream pattern. To make sure that dereddening the photometry with the map from Schlegel et al. (1998) is appropriate for this region, we compare the extinction to that extracted from 3D dust map (Bovy et al. 2016) by assuming the stream distance of 9.12 kpc (see CMD fitting in Section 3.1) and find that the typical difference in A_V is only $\sim$0.04 mag, meaning that the 2D dust map we used from Schlegel et al. (1998) is accurate enough. The trajectory can be well described with a second-order polynomial:

$$\alpha = 5.194 \times 10^{-3}\delta^2 + 4.685 \times 10^{-2}\delta + 146.141 \quad (3)$$

with $-13° < \delta < 14°$.

To estimate the stream's width, we create a mask as shown with the left green window in the middle panel of Figure 1. Here δ is between $-3°$ and $8°$, and this segment corresponds to the most prominent portion of the detected features. The boundaries on the left and right sides are parallel to Equation (3) and separated by 0°.8 (the mask's width). We then move the mask across the stream from left to right and sum all weights of stars fainter than $G = 18$ mag in the mask (again, to reduce large noises caused by bright stars) to create a one-dimensional stream profile as shown with the red solid line in the left panel of Figure 2. This is directly analogous to the T statistic of Grillmair (2009). In Figure 2, the stream is almost enclosed within $-2° <$ offset $< 2°$, and its peak is 14.88σ above the background noise outside this range. From the profile, we find an estimate of its width (full width at half maximum) to be $\sim$1°.9.

Furthermore, we create the lateral profile of unweighted stars in the same way and overplot it with the blue dashed line in the left panel of Figure 2. There is a gradient in the distribution of stars along the offset, with more stars populating at the lower offset (near the disk). It can be concluded that the stream signature is not caused by contamination of the Milky Way's field population. Otherwise, it is more likely to detect strong signals close to the offset = $-6°$ side.

Following the same way, the stream's longitudinal profile can be obtained using the bottom mask (5° by 1°.6) in Figure 1, by moving it along the decl. As displayed in the right panel of Figure 2, the red solid and blue dashed lines are presenting the same meaning as those of the left panel. From the profile of the weights, several gaps are found at, for example, $\delta \sim -5°$, $2°$, and $9°$, which also appear obvious in Figure 1. This kind of signature may suggest a result of noncontinuous stripping (Grillmair 2011) or collisions with massive perturbers in the Milky Way (Bonaca et al. 2019).

3.1. CMD and PMs

We display a background-subtracted binned CMD for the stream in the left panel of Figure 3. The stream region is defined as the area around the trajectory (Equation (3)) $\pm 1°$ in α direction, given the derived width of 1°.9. The background is estimated through averaging two offstream regions parallel to the stream obtained by moving the stream region along the α-axis by $\pm 3°$ to eliminate the effect of the gradient. Before background subtraction, a PM selection is applied to both the stream and offstream regions as illustrated with the red polygon in the right panel of Figure 3, which corresponds to the stream's distribution in the PM space (see below). We emphasize that this is a subtraction of star numbers, not weighted counts.

---

[5] These ranges and steps might be adjusted depending on specific goals and computational abilities.

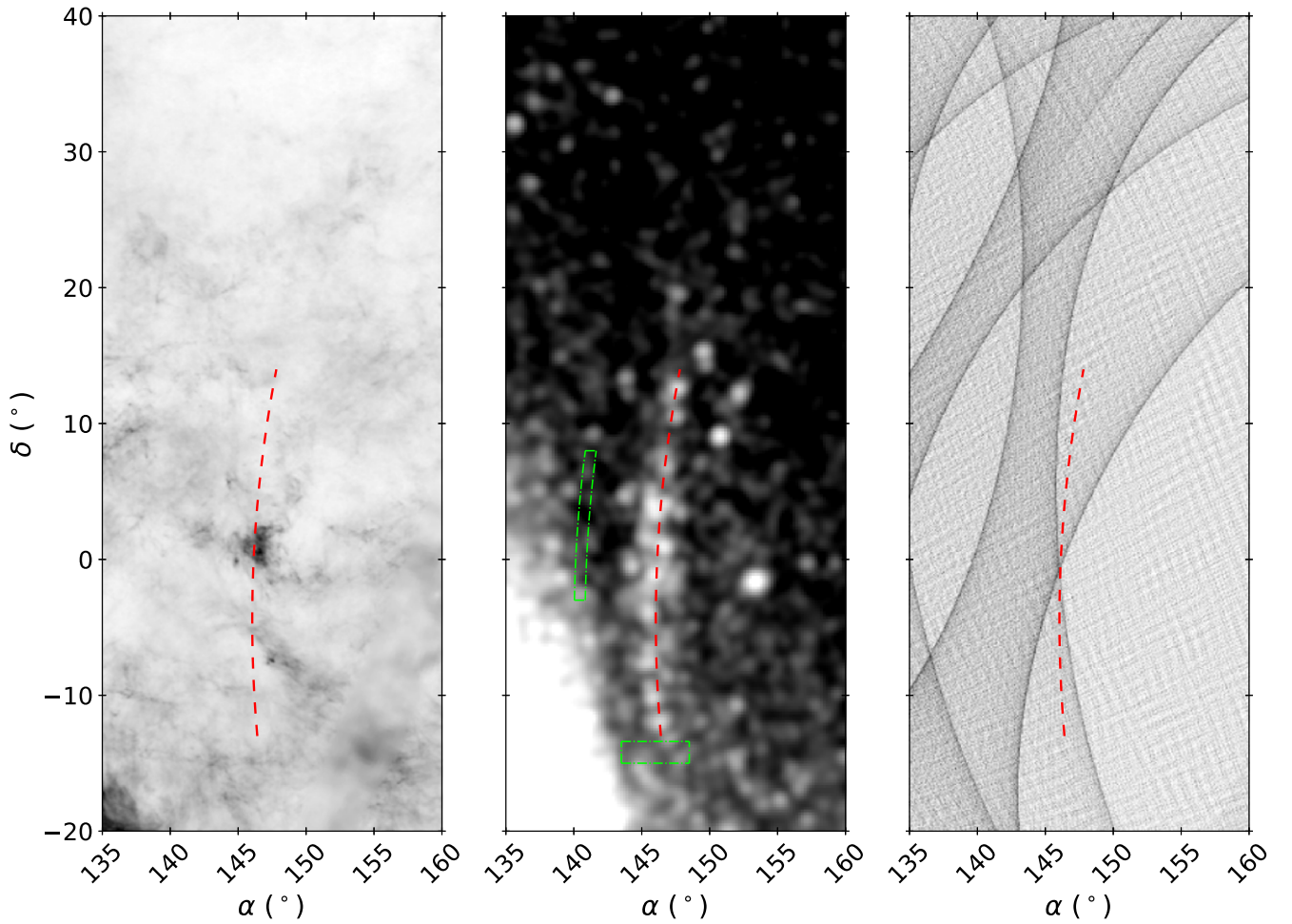[6] Its `Python` code can be found at doi:10.5281/zenodo.7604477.

Figure 1. The left and right panels present the dust extinction map extracted from Schlegel et al. (1998) and Gaia's scanning pattern covered by the DR3, respectively. The middle panel presents the weighted sky map for stars fainter than $G = 18$ mag. The green areas are two moving masks used to generate the stream's lateral and longitudinal profiles in Figure 2. The red dashed line of the three panels indicates the trajectory of the stream.
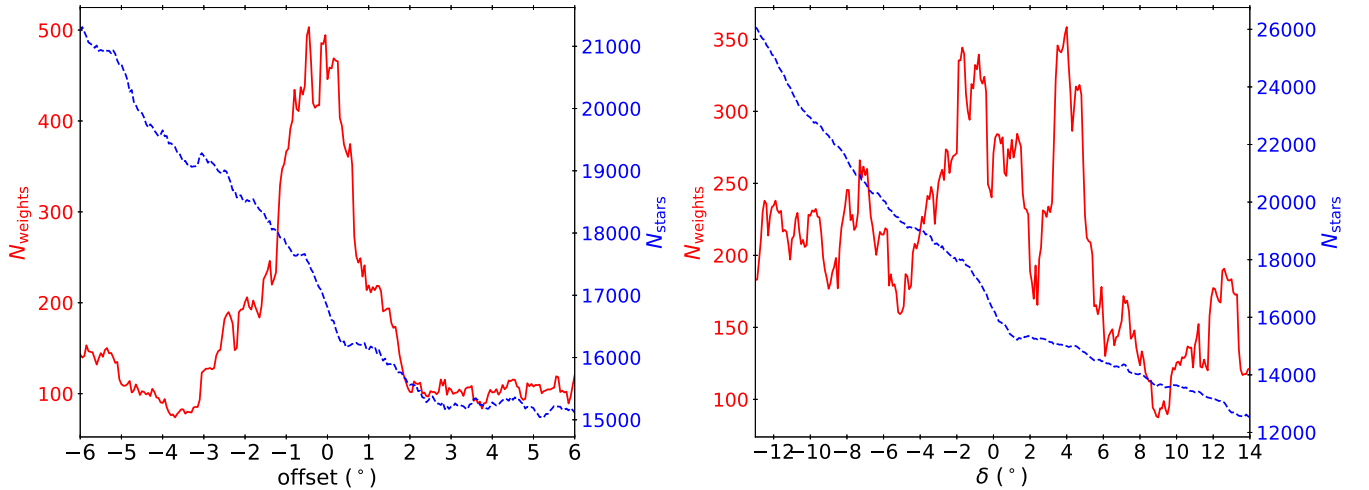

Figure 2. Left: the lateral distributions for weighted (red solid line) and unweighted (blue dashed line) numbers of stars fainter than $G = 18$ mag, obtained by moving the left mask in Figure 1 across the stream. Right: similar to the left panel but for the longitudinal profile obtained by moving the bottom mask along the stream.

The CMD bin size is 0.05 mag in color and 0.2 mag in G magnitude. The diagram is smoothed with a 2D Gaussian kernel of $\sigma = 1$ pixel. The blue dashed line represents the best-fit isochrone with age = 11 Gyr and [M/H] = -0.7 dex at $dm = 14.8$ mag. To find this best combination, we explore an isochrone grid that covers a metallicity range of $-2.2 \leqslant$ [M/H] $\leqslant -0.2$ and an age range of $10 \leqslant$ Age $\leqslant 13$ with 0.1 dex and 1 Gyr spacing, along with a dm varying from 13 to 16 with a step of 0.1 mag. The stream's strength is measured through the total weights between $-2° <$ offset $<2°$ in Figure 2, and the best-fit result is
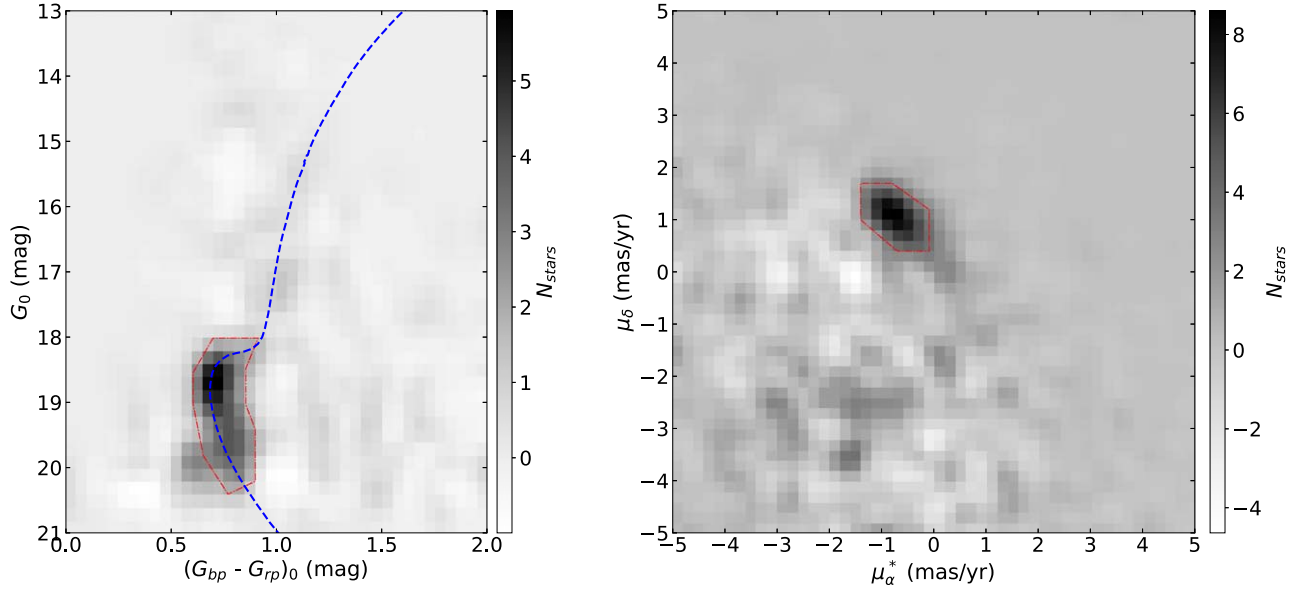
Figure 3. The left panel is a 2D histogram of stars in CMD with PMs selected and background subtracted. The blue dashed line represents the best-fit isochrone with age = 11 Gyr and [M/H] = −0.7 dex at dm = 14.8 mag. The right panel is a 2D histogram of PMs after CMD selection and background subtraction. Both of the diagrams are smoothed with a 2D Gaussian kernel of σ = 1 pixel. The red polygons represent the CMD and PM selections applied to the stream and offstream regions.

found when the stream signals become the strongest. The PM term of `StreamScanner` is fixed at (-0.4, 0.8) and (−1, 1.4) as mentioned before during this process. After the PM selection and background subtraction, the stream's main sequence along with its turnoff is clearly seen and has a good match with the isochrone. The dm = 14.8 mag corresponds to a heliocentric distance of ∼9.12 kpc. Considering the width of 1°.9, the physical width of Yangtze is about 302 pc, implying a dwarf galaxy origin.

In the right panel of Figure 3, we present a 2D histogram of PMs. Similarly, before the subtraction between the stream region and the mean of the offstream regions, a CMD selection is applied to them as shown with the red polygon in the left panel. The diagram with bin size = 0.2 mas yr^{-1} is also smoothed using a 2D Gaussian with σ = 1 pixel. An overdensity at $\mu_\alpha^* \sim -0.7$ mas yr^{-1} and $\mu_\delta \sim 1.1$ mas yr^{-1} is discernible corresponding to the stream.

We further estimate the stream's surface density and brightness. There are a total of 296 stars within the PM polygon after the background subtraction. This serves as an estimate to the number of stream stars located in a 27° × 2° region. Thus the surface density is roughly 5.5 stars deg^{-2}. For all stars in the stream region, each one is assigned a weight by `StreamScanner,` and this allows us to select the most likely members of the stream based on the sorting of weights. We adopt stars with weights > 1.255 as the member candidates because the criterion leaves us with 296 stars as well. By combining their individual G magnitudes, we get a surface brightness of Yangtze to be $\Sigma_G \simeq 34.85$ mag arcsec^{-2}. We can put this another way. We have 298 stars satisfying the CMD and PM selections simultaneously, which can be treated as member candidates as well. Those stars give a surface brightness of $\Sigma_G \simeq 34.95$ mag arcsec^{-2}, very close to the previous one.

3.2. Association with GCs and Streams

We aim to fit an orbit to Yangtze such that we can investigate whether it is related to any GC or known stream of

the Milky Way. We adopt a Galactic potential model used in Yang et al. (2022a, 2022b), where the halo is taken from McMillan (2017) and nonhalo components come from Pouliasis et al. (2017; model I). The position of the Sun is set as $(R_\odot, Z_\odot)$ = (8.122, 0.0208) kpc (GRAVITY Collaboration et al. 2018; Bennett & Bovy 2019), and the solar velocities are set to $(V_{R,\odot}, V_{\phi,\odot}, V_{Z,\odot})$ = (−12.9, 245.6, 7.78) km s^{-1} (Drimmel & Poggio 2018), respectively. The fit parameters are position α, δ, heliocentric distance d, PMs μ_α^*, μ_δ, and radial velocity V_r. We chose to anchor the decl. at $\delta = 0°$, near the midpoint of the stream, leaving other parameters free to be varied. In a Bayesian framework, sky positions and PMs of the 298 member candidates are used to constrain the parameters, and the fitted results can be derived from their marginalized posterior distributions through a Markov Chain Monte Carlo sampling. We have crossmatched these candidates with spectroscopic catalogs like LAMOST or SDSS, but unfortunately no common stars are found; thus no radial velocities are available. The best-fit parameters are $\alpha = 146.14^{+0.06}_{-0.06}$ °, $d = 8.58^{+0.39}_{-0.53}$ kpc, $\mu_\alpha^* = -0.76^{+0.02}_{-0.02}$ mas yr^{-1}, $\mu_\delta = 0.96^{+0.02}_{-0.01}$ mas yr^{-1}, and $V_r = 8.78^{+5.16}_{-5.03}$ km s^{-1}. We then obtain the stream's orbit by integrating them for ±1 Gyr under the same potential.

We first examine possible connections between Yangtze and GCs by comparing their angular momenta L_z and energy $E_{\rm tot}$ as shown in the left panel of Figure 4. The positions and velocities of the GCs are taken from Vasiliev & Baumgardt (2021). We note that the stream lies rather near Palomar 1 (Pal 1) as marked by the blue triangle. Sakari et al. (2011) already showed that Pal 1 has unusual chemical characteristics including lower [α/Fe] ratios than Galactic stars of the same [Fe/H], and they concluded an extragalactic origin for Pal 1. The metallicity of Pal 1 is −0.6 dex, which is close to −0.7 dex of Yangtze although the latter is estimated by an isochrone fitting. However, Yangtze's orbit does not pass through Pal 1 as displayed in the right panel of Figure 4, and we have also verified that the cluster's orbit does not match with the stream's
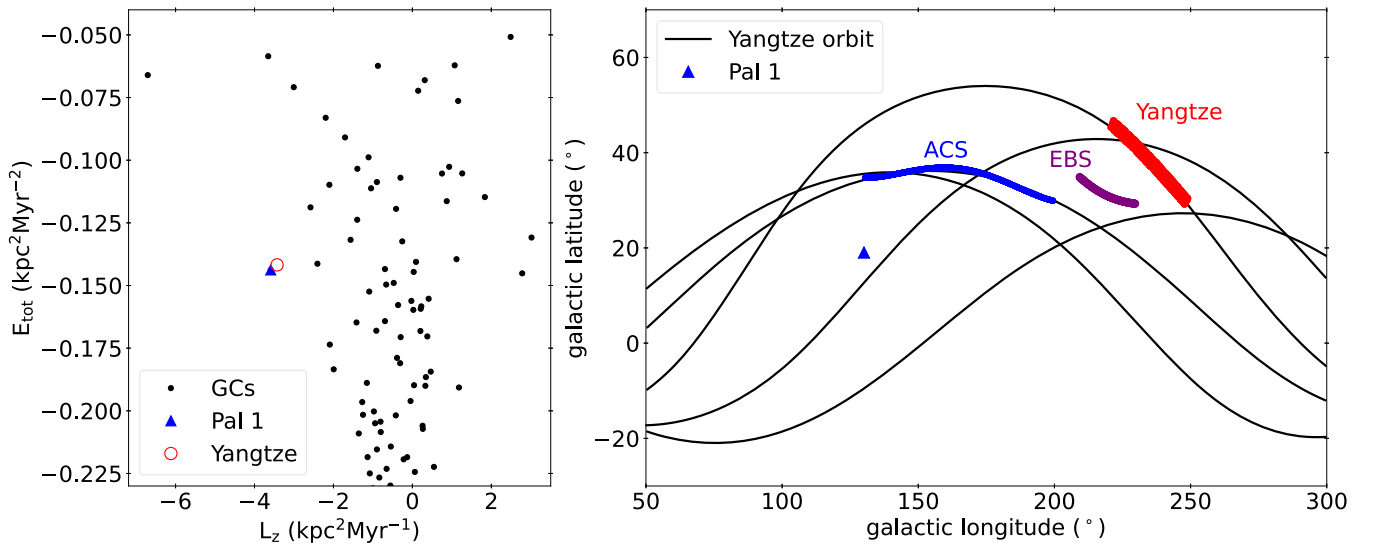
Figure 4. The left panel displays GCs (black points) and Yangtze (red circle) in angular momenta and energy space. The right panel presents projections of streams and orbits in Galactic coordinate. The red line and black lines indicate Yangtze and its best-fit orbit. The blue and purple lines represent ACS and EBS, respectively. The blue triangle denotes Pal 1.

track either. Thus it might be a better interpretation that Pal 1 is a GC brought in by the progenitor of Yangtze.

Among known streams, we find that the trajectory of the Anticenter Stream (ACS; Grillmair 2006b) matches quite well with the orbit of Yangtze as shown in the right panel of Figure 4. Here the footprint of ACS is based on the results of Ramos et al. (2021), which is extracted from the galstreams library (Mateu 2023). ACS is likely on the Yangtze's orbit though they are separated by one orbit around the Galaxy. Yangtze's pericenter and apocenter are $R_{\mathrm{peri}} = 12.1\,\mathrm{kpc}$ and $R_{\mathrm{apo}} = 18.9\,\mathrm{kpc}$, close to $R_{\mathrm{peri}} = 15.4\,\mathrm{kpc}$ and $R_{\mathrm{apo}} = 19.0\,\mathrm{kpc}$ of ACS (Grillmair et al. 2008). It is also worth noting that our metallicity estimate is nearly identical to $[\mathrm{Fe/H}] = -0.72$ dex of ACS (Zhang et al. 2022). All similarities connect these two streams and imply that they may share a common origin. Besides ACS, we also show the Eastern Banded Structure (EBS; Grillmair 2011), another substructure in the anticenter region. The three streams are located rather close and nearly parallel to one another on the sky, but for EBS and Yangtze, their inferred orbits suggest that they are dynamically distinct.

4. Conclusion

With revised photometry and astrometry from Gaia DR3, we show a new stream probably formed from a dwarf galaxy's disruption, which we dub Yangtze. The stream is detected at a significance of $\sim15\sigma$ with a StreamScanner method that assigns weights to stars in the CMD and PMs simultaneously. The Yangtze is spanning $27°$ by $1°9$ on the sky at 9.12 kpc away from the Sun. Its stellar population is well fitted with an isochrone of age = 11 Gyr and $[\mathrm{M/H}] = -0.7$ dex. The stream has a low surface brightness of $\Sigma_G \simeq 34.9$ mag arcsec^{-2}, with a density of about 5.5 stars deg^{-2}. We also demonstrate that Yangtze may be associated with ACS and Pal 1, and we suspect that these two streams are remnants of one dwarf galaxy that brought the cluster into the Milky Way. Spectroscopic observations will be required to give deeper insights to it.

ORCID iDs

Yong Yang ⓘ https://orcid.org/0000-0001-7609-1947
Jing-Kun Zhao ⓘ https://orcid.org/0000-0003-2868-8276
Xian-Hao Ye ⓘ https://orcid.org/0000-0002-5805-8112
Gang Zhao ⓘ https://orcid.org/0000-0002-8980-945X
Ke-Feng Tan ⓘ https://orcid.org/0000-0003-0173-6397

References

Antoja, T., Helmi, A., Romero-Gómez, M., et al. 2018, Natur, 561, 360
Bennett, M., & Bovy, J. 2019, MNRAS, 482, 1417
Bonaca, A., Hogg, D. W., Price-Whelan, A. M., & Conroy, C. 2019, ApJ, 880, 38
Bovy, J., Rix, H.-W., Green, G. M., Schlafly, E. F., & Finkbeiner, D. P. 2016, ApJ, 818, 130
Bressan, A., Marigo, P., Girardi, L., et al. 2012, MNRAS, 427, 127
Chang, J., Yuan, Z., Xue, X.-X., et al. 2020, ApJ, 905, 100
Drimmel, R., & Poggio, E. 2018, RNAAS, 2, 210
Gaia Collaboration, Brown, A. G. A., Vallenari, A., et al. 2021, A&A, 649, A1
GRAVITY Collaboration, Abuter, R., Amorim, A., et al. 2018, A&A, 615, L15
Grillmair, C. J. 2006a, ApJL, 645, L37
Grillmair, C. J. 2006b, ApJL, 651, L29
Grillmair, C. J. 2009, ApJ, 693, 1118
Grillmair, C. J. 2011, ApJ, 738, 98

Grillmair, C. J. 2019, ApJ, 884, 174
Grillmair, C. J., & Carlin, J. L. 2016, in Tidal Streams in the Local Group and Beyond, Astrophysics and Space Science Library, Vol. 420, ed. H. J. Newberg & J. L. Carlin (Cham: Springer), 87
Grillmair, C. J., Carlin, J. L., & Majewski, S. R. 2008, ApJL, 689, L117
Helmi, A., Babusiaux, C., Koppelman, H. H., et al. 2018, Natur, 563, 85
Ibata, R. A., Gilmore, G., & Irwin, M. J. 1994, Natur, 370, 194
Ibata, R., Malhan, K., Martin, N., et al. 2021, ApJ, 914, 123
Law, D. R., & Majewski, S. R. 2010, ApJ, 714, 229
Li, T. S., Simon, J. D., Kuehn, K., et al. 2018, ApJ, 866, 22
Liang, X. L., Zhao, J. K., Oswalt, T. D., et al. 2017, ApJ, 844, 152
Lindegren, L., Klioner, S. A., Hernández, J., et al. 2021, A&A, 649, A2
Malhan, K., Yuan, Z., Ibata, R. A., et al. 2021, ApJ, 920, 51
Mateu, C. 2023, MNRAS, in press
McMillan, P. J. 2017, MNRAS, 465, 76
Newberg, H. J., Yanny, B., & Willett, B. A. 2009, ApJL, 700, L61
Pouliasis, E., Di Matteo, P., & Haywood, M. 2017, A&A, 598, A66
Ramos, P., Antoja, T., Mateu, C., et al. 2021, A&A, 646, A99
Re Fiorentin, P., Spagna, A., Lattanzi, M. G., & Cignoni, M. 2021, ApJL, 907, L16
Riello, M., De Angeli, F., Evans, D. W., et al. 2021, A&A, 649, A3
Sakari, C. M., Venn, K. A., Irwin, M., et al. 2011, ApJ, 740, 106
Schlafly, E. F., & Finkbeiner, D. P. 2011, ApJ, 737, 103
Schlegel, D. J., Finkbeiner, D. P., & Davis, M. 1998, ApJ, 500, 525
Vasiliev, E., & Baumgardt, H. 2021, MNRAS, 505, 5978
Yang, Y., Zhao, J.-K., Ishigaki, M. N., et al. 2022a, A&A, 667, A37
Yang, Y., Zhao, J.-K., Ishigaki, M. N., et al. 2022b, MNRAS, 513, 853
Yang, Y., Zhao, J.-K., Xue, X.-X., Ye, X.-H., & Zhao, G. 2022c, ApJL, 935, L38
Yang, Y., Zhao, J., Zhang, J., Ye, X., & Zhao, G. 2021, ApJ, 922, 105
Ye, X., Zhao, J., Zhang, J., Yang, Y., & Zhao, G. 2021, AJ, 162, 171
Yuan, Z., Chang, J., Beers, T. C., & Huang, Y. 2020, ApJL, 898, L37
Zhang, Z., Shi, W. B., Chen, Y. Q., et al. 2022, ApJ, 933, 151
Zhao, G., & Chen, Y. 2021, SCPMA, 64, 239562
Zhao, J. K., Ye, X. H., Wu, H., et al. 2020, ApJ, 904, 61
Zhao, J. K., Zhao, G., Aoki, W., et al. 2018, ApJ, 868, 105
Zhao, J., Zhao, G., & Chen, Y. 2009, ApJL, 692, L113